Biomimetic Sensor Suite for Flight Control of a Micromechanical Flying Insect: Design and Experimental Results

Wei-Chung Wu Luca Schenato Robert J. Wood Ronald S. Fearing

Department of Electrical Engineering and Computer Sciences
University of California, Berkeley, CA 94720
{*wcwu, lusche, rjwood, ronf*}*@robotics.eecs.berkeley.edu*

***Abstract*—Four prototypes of biomimetic sensors have been designed and implemented for flight control of a robotic flying insect. The ocelli use four photodiodes to detect changes in light intensity in the surrounding. The halteres use piezo-actuated vibrating structures to sense body rotational velocities via the Coriolis forces. The optic flow sensors consist of linear arrays of elementary motion detectors (EMDs) to register optic flows. The magnetic field sensor uses three metal loops to detect changes in the magnetic field. Despite simplicity and novelty, the preliminary tests on these devices showed promising performance for using such biomimetic sensors on a robotic flying insect.**

I. Introduction

Micro aerial vehicles (MAVs) have drawn a great deal of attention in the past decade due to the quick advances in microtechnology and several groups have worked on MAVs based on fixed and rotary wings [1]. However, flapping flight provides superior maneuverability that would be beneficial in obstacle avoidance and for navigation in small spaces. The UC Berkeley Micromechanical Flying Insect (MFI) project uses biomimetic principles to develop an inch-size, flapping-winged robot that will be capable of sustained autonomous flight [2][3].

The MFI will be equipped with different types of sensors that are important for stabilizing flight as well as navigation. Because of the limited size and power budget available to the MFI, the designs (package size, power requirements, *etc*.) of commercially available micro sensors are in general not suitable for the MFI. On the other hand, novel biomimetic devices based on the sensory systems of real insects are considered. In particular, ocelli, halteres, optic flow sensors, and magnetic field sensors have been designed and implemented. The ocelli are used to estimate body attitude relative to a fixed frame. The halteres are used to measure body rotational velocities. The optic flow sensors are used to avoid objects in the flight course as well as for stabilization. The magnetic field sensors are used to adjust an insect's heading. These devices have the virtues of simple design, easy implementation, low power consumption, and high performance. This paper presents the designs, simulations, and experimental results of these biologically inspired sensing devices.

This work was funded by ONR MURI N00014-98-1-0671 and DARPA.

II. Ocelli

The ocelli are light-sensitive organs present in most flying insects. This system consists of three wide angle photoreceptors on the head of an insect. They are oriented in such a way that they collect light from different regions of the sky (see Fig. 1). Albeit the exact physiology of the ocelli and their scope in insect flight are still not completely unveiled, it is believed that they play a fundamental role in attitude stabilization, in particular, in horizon stabilization [4][5].

Biologists believe that ocelli estimate the orientation of the insect with respect to the sky by comparing the intensity of light measured by the different photoreceptors. Their argument is based on the assumption that, as a first approximation, the intensity of light, I, measured by the photoreceptors is only a function of its latitude relative to the light source (*i.e.* the sun). In our implementation, we use four photodiodes for the ocelli system. Although real insects have three ocelli, we prefer a four-receptor config-

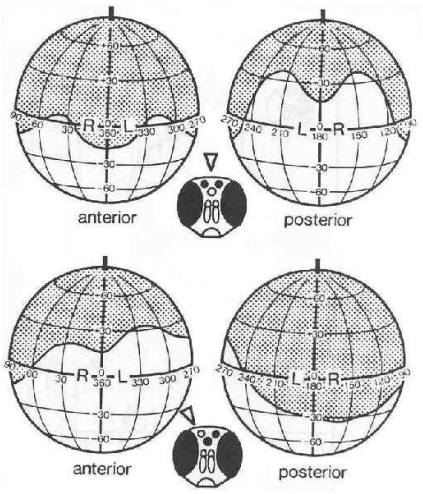

Fig. 1. The ocelli of a blowfly and the visual fields of the median (top) and right lateral (bottom) ocelli. Courtesy of [5].

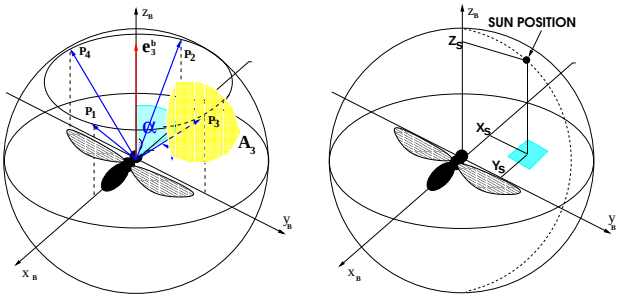

Fig. 2. (a) Four photoreceptors, P_1, P_2, P_3, and P_4, are fixed with respect to the insect's body frame (x_B, y_B, z_B). The shadowed area, A_3, represents the receptive region of P_3; (b) The projection of the light source onto the $x-y$ plane of the insect's body frame. The shadowed area represents the box given by (3).

uration because the design is simplified and the results are intuitive. Also, our concept can be easily extended to the three-receptor case.

Four ideal photoreceptors, P_1, P_2, P_3, and P_4, are fixed with respect to the body frame, B, of an insect. They are oriented symmetrically such that they have the same latitude and their axes intersect the sky sphere forming an imaginary pyramid whose vertex is placed at the center of the insect's head. Formally, their orientations relative to the body frame, B, can be represented in Cartesian coordinates as follows:

$$\begin{array}{l} P_1^b = [\sin\alpha\ 0\ \cos\alpha]^T,\ P_2^b = [-\sin\alpha\ 0\ \cos\alpha]^T \\ P_3^b = [0\ \sin\alpha\ \cos\alpha]^T,\ P_4^b = [0\ -\sin\alpha\ \cos\alpha]^T \end{array} \quad (1)$$

where the parameter, $\alpha \in (0, \pi)$, sets the latitude of the photoreceptors. Each photoreceptor collects light from a conic region, A_i, of the sky around its orientation P_i as shown in Fig. 2.

The measurements from the photoreceptors are simply subtracted pairwise and these two signals are the output from the ocelli:

$$\begin{array}{rcl} s_1 & = & I(P_1) - I(P_2) \\ s_2 & = & I(P_3) - I(P_4) \end{array} \quad (2)$$

where $I(P_i)$ is the output from the i^{th} photodiode. If the output of a photodiode is a *monotonically decreasing* function of its latitude relative to the light source, we have the following proposition:

Proposition 1. *If the photoreceptor output is a monotonically decreasing function of its latitude, $\theta_i \in [0, \pi]$, relative to the light source, then the signals, s_1 and s_2, defined in (2) always satisfy the following conditions:*

$$\begin{array}{l} \underline{k} x_s \le s_1 \le \bar{k} x_s \\ \underline{k} y_s \le s_2 \le \bar{k} y_s \end{array} \quad (3)$$

where $0 < \underline{k} < \bar{k}$ are constants, and x_s and y_s are, respectively, the x and y projections of the light source on the $x-y$ plane of the ocelli.

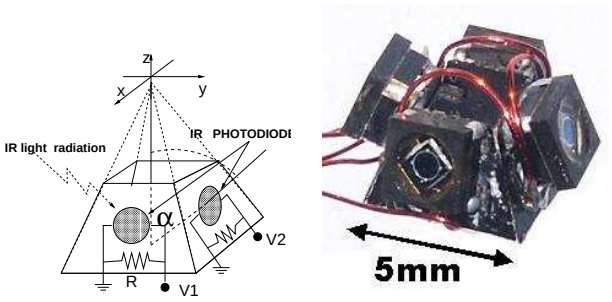

Fig. 3. (a) Schematic of ocelli design; (b) Photo of the ocelli structure.

It is evident that the output from the ocelli can be used as an estimate of the orientation of the ocelli reference frame relative to the light source. Thus, they can be used to align the ocelli reference frame with the light source as described in detail in [6].

Based on the mathematical modeling, we have designed a biomimetic ocelli system. The device has four IR photodiodes soldered onto a pyramid as shown in Fig. 3. Each photodiode collects light radiation, which induces electric current that is proportional to the intensity of light collected and the active area of the photodiode. Each photodiode is placed in parallel with a small resistor and the voltage drop across the resister is measured. The output voltages from the four photodiodes are combined differentially to give the two ocelli outputs, which are used as estimators of light source orientation:

$$\begin{array}{rcl} s_1 & = & V_1 - V_3 \\ s_2 & = & V_2 - V4 \end{array} \quad (4)$$

To test the sensitivity and output range of the ocelli sensors, the devices are allowed to move in a $6 \times 8cm$ region centered at the origin $O = (0, 0, 0)$. An IR lamp is positioned at $P_S = (0, 0, h)$, where $h \approx 10cm$ is the height from the plane of the ocelli to the light source. The orientation of the pyramid is kept constant such that the photodiodes 1 and 3 are parallel to the x-axis, while 2 and 4 are parallel to the y-axis. Then, the ocelli are moved to different $x-y$ positions and the recorded output signals are shown in Fig. 4. The ocelli output gives an excellent estimate of the distance from the ocelli structure to the origin. Among the structures tested, the pyramid with angle $\alpha = 40^o$ shows the best performance in terms of range and linearity with distance. The measurements did not need any kind of noise filtering and the results were repeatable. The size of the whole structure is about $5 \times 5 \times 5mm$ and it weighs $150mg$. However, the size and weight can be further reduced if bare photodiodes are used since the active area of one photodiode is $0.73mm^2$.

III. HALTERE

Estimation of angular velocities in aerial vehicles is fundamental for flight stabilization and maneuvering. Re-

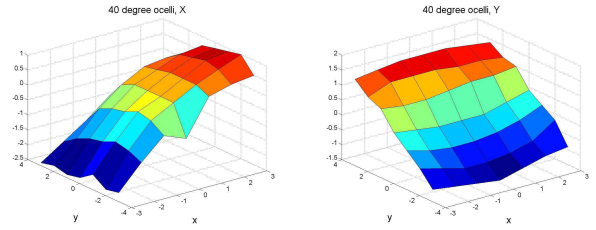

Fig. 4. s_1 (left) and s_2 (right) measurements for ocelli structure with $\alpha = 40^o$.

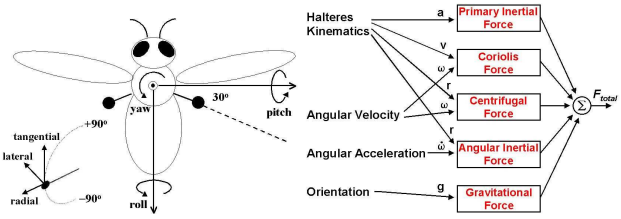

Fig. 5. (a) Schematic of the halteres; (b) Components of the force acting on the haltere.

search on insect flight revealed that insects use structures, called halteres, to measure body rotational velocities via gyroscopic forces [7]. The halteres of a fly resemble small balls at the end of thin rods. During flight the halteres beat up and down through an angle of nearly 180^o anti-phase to the wings at the wingbeat frequency. Additionally, the two halteres are non-coplanar (see Fig. 5a). This non-coplanarity of the two halteres is essential for a fly to detect rotational velocities about all three turning axes [8].

As a result of insect motion and haltere kinematics, a complex force acts on the halteres during flight:

$$\mathbf{F} = m\mathbf{g} - m\mathbf{a} - m\dot{\boldsymbol{\omega}} \times \mathbf{r} - m\boldsymbol{\omega} \times (\boldsymbol{\omega} \times \mathbf{r}) - 2m\boldsymbol{\omega} \times \mathbf{v} \quad (5)$$

where m is the mass of the haltere, $\mathbf{r}$, $\mathbf{v}$, and $\mathbf{a}$ are the position, velocity, and acceleration of the haltere relative to the insect body, $\boldsymbol{\omega}$ and $\dot{\boldsymbol{\omega}}$ are the angular velocity and angular acceleration of the insect, and $\mathbf{g}$ is the gravitational constant (see Fig. 5b). Among the force components in (5), only the centrifugal ($-m\boldsymbol{\omega} \times (\boldsymbol{\omega} \times \mathbf{r})$) and Coriolis ($-2m\boldsymbol{\omega} \times \mathbf{v}$) components depend on the insect's angular velocity. However, the centrifugal force is proportional to the square of angular velocity of the insect, it provides no information on the sign of rotations. The Coriolis force, on the other hand, is used because it contains information on the axis, sign, and magnitude of the insect's angular velocity. In order to retrieve this Coriolis component, the force signals orthogonal to a haltere's beating plane are measured because all other interfering force components are small in this direction. Further, because the Coriolis force is dependent on the haltere velocity, these signals are modulated in time with the haltere beat frequency. Thus, utilizing the characteristics (frequency, modulation, and phase) of the Coriolis signals on the left and right halteres, a demodulation scheme has been proposed to decipher roll, pitch, and yaw rotations [9].

Since a haltere must have only one sensing degree of freedom ($i.e.$ the direction orthogonal to the haltere beating plane), the design of a mechanical haltere must allow for high stiffness in the tangential direction and compliance in the lateral direction. The best case mechanically for this is a flat beam with the wide face in the plane of the haltere beating and the end of the beam is twisted to allow a high Q compliant section for rotation as in Fig. 6a. To detect the Coriolis forces, two strain gauges are placed, one on either side of the beam, close to the point of rotation such that one would be in compression while the other is in tension. In addition, because the Coriolis forces are proportional to the haltere velocity, it is desired to have a high haltere beat frequency and a large stroke. This can be achieved by placing the haltere on the output link of a fourbar mechanism driven by a piezoelectric actuator, similar to the method used to drive the MFI wing as described in [2] [3]. Fig. 6b shows the completed haltere.

The test results for the haltere under rotations about the longitudinal axis of the structure are seen in Fig. 7. With the fourbar driven structure, the position of the haltere can be sensed using actuator-mounted strain sensors as described in [10]. This haltere position is normalized to yield a unity magnitude $sine$ wave which represents the haltere phase. This is then used to demodulate the force signals using the proposed demodulation scheme. The performance of the haltere shows some key features for use on the MFI. First, the haltere needs very little power since it can be driven parasitically from the body vibrations of the MFI. Second, the haltere has a large dynamic range to accommodate slow turns as well as saccades (90^o turns in less than $100ms$). Finally, when the wings of the MFI are flapping, the wing inertia will cause the MFI body to oscillate along the axis parallel to the stroke direction. The haltere can reduce the error caused by these common-mode oscillations by phase-locking to the wing.

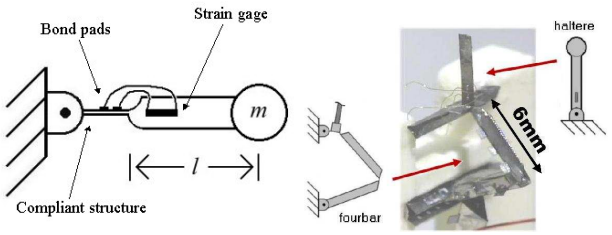

Fig. 6. (a) Haltere design parameters; (b) Photo of the completed haltere on a fourbar structure. Adapted from [9].

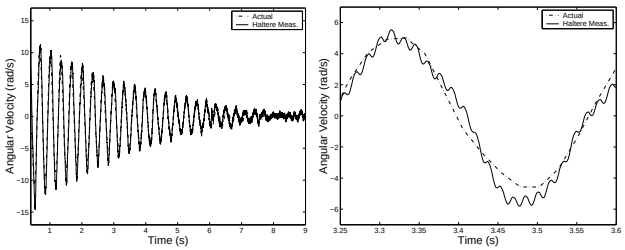

Fig. 7. (a) Result for the fourbar actuated haltere; (b) Zoomed in to show accuracy. Adapted from [9].

IV. Optic Flow Sensor

Studies of insect's visual behaviors found that when a fly is presented with a leftward (or rightward) moving stimulus, it would turn in the direction of stimulus movement in order to reduce the image motion on its eyes. Such a response is believed to help the fly maintain a straight course by compensating for undesired deviations during flight [11]. Hassenstein and Reichardt proposed a motion detection mechanism using the spatiotemperal elements of image motion [12]. This type of correlation-based algorithm represents an adequate model of the signal transduction pathway in a fly's visual system.

The building block of the Reichardt motion sensor is an elementary motion detector (EMD) whose structure is shown in Fig. 8a. When a moving image is presented to an EMD, the perceived signal in one receptor is compared to the delayed signal in a neighboring receptor. If the left signal correlates more strongly to the delayed right signal, then the image is moving from right to left and vice versa. In the EMD implementation, the bandpass filter represents the temporal frequency response of the photoreceptor. The lowpass filter provides the delay operation and the multiplication achieves the correlation required by the EMD. The opponent subtraction results in different signs for the leftward and rightward image motions. Because an EMD can not detect image motion that is perpendicular to the transverse axis of the two receptors, two EMDs in a cross configuration are used to detect image motion in orthogonal directions. Fig. 8b shows the completed structure of the EMDs. Similar to the ocelli, the size and weight of the device can be reduced if bared photodiodes are used. Moreover, the photodiodes are most sensitive to light at a wavelength of $880nm$ and have an optimal receptive field of approximately 45^o. This large receptive field of individual photodiodes offsets the low spatial acuity due to the large separation between the two photodiodes.

Image motions seen by an insect's eyes are encoded by the perceived optic flows. Higher image motions result in greater optic flows. Therefore, when an insect flies toward an object, the quick expansion of that object in the insect's visual field would induce large optic flows across its eyes. This kind of flow signals can be exploited to perform tasks

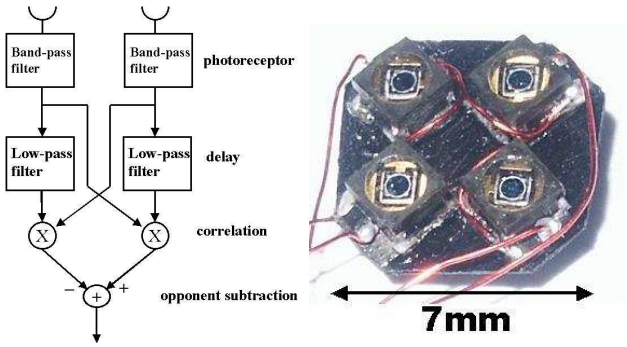

Fig. 8. (a) Elementary motion detector architecture; (b) Photo of two EMDs oriented in orthogonal directions.

such as obstacle avoidance and terrain tracking. In the simulation, a one-dimensional flow sensor consisting of an array of twenty EMDs is used for a fly to follow a simple topography of the ground (see top panel of Fig. 9). A flow sensor is placed on the head of the fly and is tilted downward by 60^o. The bottom panel shows the accumulated optic flows perceived by the sensor during the flight. When the fly is closer to the ground, the patterns on the ground cause the optic flows to increase quickly. An upper threshold for the perceived optic flows is set such that when this value is reached the fly would elevate in order to maintain a safe distance to the ground. On the other hand, when the fly is at a higher position, the patterns on the ground do not induce significant optic flows and hence the accumulated signals decrease. Accordingly, the fly would descend when a preset lower threshold is reached. By choosing appropriate upper and lower threshold values, the fly can follow the topography of the ground properly.

Ideally a flow sensor would contain many EMDs whose outputs are summed to eliminate oscillations that are present in the output of a single EMD. Although our sensor

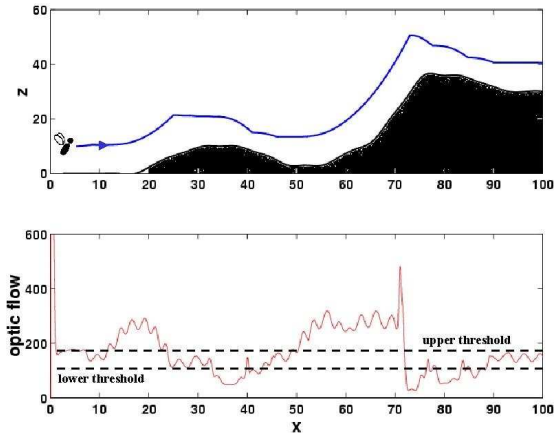

Fig. 9. The fly follows the topography of the ground (top) based on the perceived optic flow (bottom) during the flight.

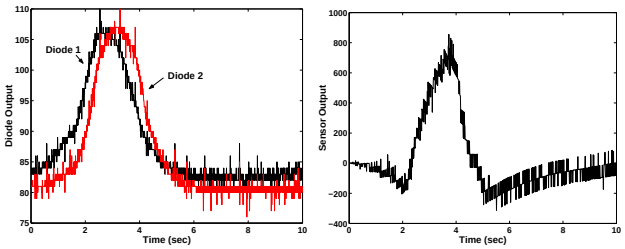

Fig. 10. (a) Output from photodiodes 1 and 2; (b) Output from the one-dimensional EMD.

consists of only one EMD (two photodiodes) in either direction of the device and its output exhibits the expected oscillations, the purpose of our sensor is to detect optic flows induced by objects when the MFI is moving. To test our flow sensor, we shined IR light on a piece of white paper with a black stripe on it. Then, we slowly moved the sensor across the paper and recorded the outputs from both photodiodes. The results are shown in Fig. 10a. The outputs of these two photodiodes are further processed by the delay-and-correlate operation and the result is given in Fig. 10b. It is obvious that with only two photodiodes, our sensor can still register optic flows.

V. Magnetic Field Sensor

Control of the MFI body attitude requires a set of sensors that can estimate its orientation relative to a fixed frame. The ocelli system provides a means to reorient the insect body towards a specific direction, however, the insect's heading remains arbitrary. Since heading is important for forward flight and maneuvering, we propose using a magnetic field sensor for the MFI. This magnetic sensor can estimate the heading based on the terrestrial geomagnetic field. The magnetic sensor is a U-shaped suspended structure (see Fig. 11a), similar to that proposed in [13]. Electric current flows through this structure, interacting with the terrestrial geomagnetic field, and induces the Lorentz force:

$$F = LIB\sin\alpha \tag{6}$$

where F is the total force at the tip of the cantilever, L is the length of one loop, I is the total current, B is the terrestrial electromagnetic field, and α is the angle between the direction of the magnetic field and the electric current. The deflection of the cantilever, which is proportional to the force perpendicular to the cantilever, is sensed at the base by strain gauges whose output can be used to estimate the heading of the MFI. Given the stringent requirements imposed by the MFI design, this magnetic sensor needs to have a small size $L < 20mm$, a resolution $\delta\alpha < 1^o$ for $-60^o < \alpha < 60^o$, a large bandwidth $f > 2kHz$, and small power consumption $P < 2mW$. These requirements relate to the geometric design variables as follows:

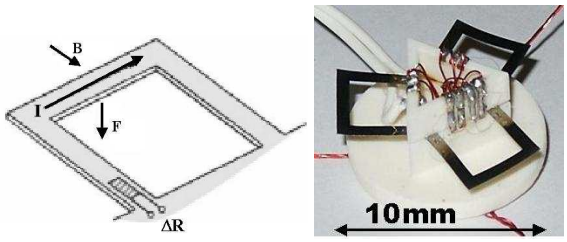

Fig. 11. (a) Schematic of a magnetic sensor design; (b) Photo of the magnetic sensor with three metal loops.

$$\begin{aligned} \delta\alpha &= \frac{180Ewt^2\epsilon_{min}}{9\pi BL^2I} \\ f &= \frac{1}{4\pi L}\sqrt{\frac{3Et}{14\rho}} \\ P &= \frac{3I^2\varrho L}{wt} \end{aligned} \tag{7}$$

where E is the Young's modulus of stainless steel, w is the width of the cantilever beam, t is the thickness, ϵ_{min} is the minimum sensitivity of the strain gauge, ρ is the density of stainless steel, and ϱ is the resistivity of stainless steel. Since there are several performance metrics that can be chosen, we tried to optimize the sensor sensitivity while satisfying the constraints on size, power consumption, and bandwidth. Moreover, electric current and beam thickness were fixed, while cantilever width and length were the design variables. Fig. 12 shows performance variables as a function of cantilever width and length. Table I shows the optimal width and length and the predicted performance in terms of desired resolution, power consumption, and bandwidth. These design specifications show feasibility since they satisfy the stringent requirements imposed by the MFI design, while provide a simple way to estimate the heading of the MFI. Fig. 11b shows the completed magnetic sensor. The three metal sections of this sensor are $12.5\mu m$ stainless steel which were laser micromachined into the desired

TABLE I
FIXED PARAMETERS ARE ON TOP AND OPTIMIZED VARIABLES ARE AT BOTTOM.

Parameter	Value	Unit
ρ	8,000	Kg/m^3
ϵ_{min}	10^{-7}	
E	193	GPa
I	1	mA
t	12.5	μm
ϱ	$7.2 \cdot 10^{-3}$	Ω/m
B	50	μT
L	8	mm
w	60	μm
f	6.3	kHz
$\delta\alpha$	1	deg
P	1.45	mW

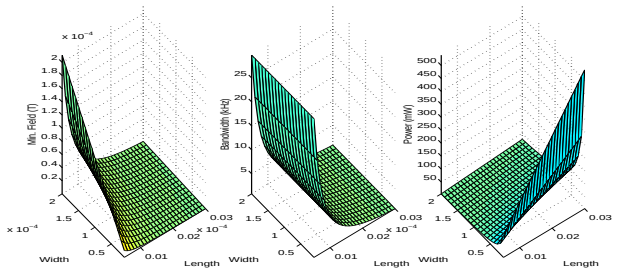

Fig. 12. Minimum detectable magnetic field (left), bandwidth (middle) and power dissipation (right) of the magnetic sensor as a function of length and width of a cantilever.

shape. The surface of the stainless steel was coated with a thin insulating layer, and semiconductor strain gauges were fixed to the base of the three sections using an automated micro-assembly stage [14][15].

VI. Conclusions and Future Work

In this paper we presented the sensory system for the MFI. It consists of four biomimetic devices: ocelli, haltere, optic flow sensor, and magnetic field sensor, which are essential for the MFI to maintain stable flight as well as achieve simple maneuvering. Although high precision micro sensors are available, they generally do not meet the stringent requirements of MAVs as small as the MFI. The design of our devices has taken into account the size, power budget, and computational power of the MFI while still be able to show high performance. Moreover, our devices can be further improved without significant revisions of their structures. In the future, these sensors will be integrated to the flight mill, an apparatus that demonstrates simplified aerodynamics of flapping flight, in order to investigate their performance as a whole sensory system and test different flight control techniques using output feedback from this sensory system.

References

[1] B. Motazed, D. Vos, and M. Drela. Aerodynamics and flight control design for hovering MAVs. In *Proc of Amer Control Conference*, Philadelphia, PA, June 1998.

[2] R.S. Fearing, K.H. Chiang, M.H. Dickinson, D.L. Pick, M. Sitti, and J. Yan. Wing transmission for a micromechanical flying insect. In *Proc of the IEEE Int'l Conf on Robotics and Automation*, pages 1509–1516, San Francisco, CA, April 2000.

[3] J. Yan, R.J. Wood, S. Avadhanula, R.S. Fearing, and M. Sitti. Towards flapping wing control for a micromechanical flying insect. In *Proc of the IEEE Int'l Conf on Robotics and Automation*, pages 3901–3908, Seoul, South Korea, May 2001.

[4] R.G. Kastberger. The ocelli control the flight course in honeybees. *Physiological Entomology*, 15:337–346, 1990.

[5] H. Schuppe and R. Hengstenberg. Optical properties of the ocelli of calliphora erythrocephala and their role in the dorsal light response. *Journal of Comparative Biology A*, 173:143–149, 1993.

[6] L. Schenato, W.C. Wu, and S. Sastry. Attitude control for a micromechanical flying insect via sensor output feedback. In *The 7th Int'l Conf on Control, Automation, Robotic and Vision*, Singapore, Dec 2002.

[7] R. Hengstenberg. Mechanosensory control of compensatory head roll during flight in the blowfly Calliphora erythrocephala Meig. *Journal of Comparative Physiology A*, 163:151–165, 1988.

[8] G. Nalbach. The halteres of the blowfly Calliphora: I. kinematics and dynamics. *Journal of Comparative Physiology A*, 173:293–300, 1993.

[9] W.C. Wu, R.J. Wood, and R.S. Fearing. Halteres for the micromechanical flying insect. In *Proc of the IEEE Int'l Conf on Robotics and Automation*, Washington, DC, May 2002.

[10] R.J. Wood and R.S. Fearing. Flight force measurement for a micromechanical flying insect. In *Intelligent Robots and Systems*, Maui, HI, 2001.

[11] M.V. Srinivasan, M. Poteser, and K. Kral. Motion detection in insect orientation and navigation. *Vision Research*, 39:2749–2766, 1999.

[12] W. Reichardt. *Autocorrelation, a principle for relative movement discrimination by the central nervous system*. MIT Press, New York, 1961.

[13] V. Beroulle, Y. Bertrand, L. Latorre, and P. Nouet. Test and testability of a monolithic mems for magnetic field sensing. *Journal of Electronic Testing: Theory and Applications*, 17:439–50, 2001.

[14] J.A. Thompson and R.S. Fearing. Automating microassembly with ortho-tweezers and force sensing. In *Intelligent Robots and Systems*, Maui, HI, 2001.

[15] R. Sahai and R.S. Fearing. Towards automatic assembly of subcentimeter millirobot structures. In *The 3rd Int'l Workshop on Microfactories*, Minneapolis, MN, Sept 2002.